Journal of Chromatography A, 1216 (2009) 6917–6930

Contents lists available at ScienceDirect

Journal of Chromatography A

journal homepage: www.elsevier.com/locate/chroma

Characteristics of the adsorption mechanism of acido-basic compounds with two pK_a in reversed-phase liquid chromatography

Fabrice Gritti, Georges Guiochon*

Department of Chemistry, University of Tennessee, Knoxville, TN, 37996-1600, USA

ARTICLE INFO

Article history:
Received 17 February 2009
Received in revised form 27 July 2009
Accepted 28 July 2009
Available online 5 August 2009

Keywords:
HPLC of acido-basic compounds
Multi pK_a compounds
RPLC
Adsorption mechanism
X-Bridge-C_{18}
Activity coefficients
Extended Debye–Hückel theory
Methanol–water mobile phase
$^{S}_{W}$pH
Ionic strength
Langmuir adsorption isotherm
Phthalic acid
Nicotinic acid

ABSTRACT

Overloaded band profiles of phthalic acid, nicotinic acid, and sodium nicotinate eluted with a methanol-aqueous buffer solution were recorded at the exit of a 150 mm ×4.6 mm column packed with 3.5 μm X-Bridge-C_{18} porous particles. The $^{S}_{W}$pHs of the mobile phase was adjusted at different values, with addition of hydrochloric acid ($^{S}_{W}$pH∼ 1.37), phosphate ($^{S}_{W}$pH∼ 2.01, 2.85, and 7.32), formate ($^{S}_{W}$pH∼ 3.61), acetate ($^{S}_{W}$pH∼4.41 and 5.15), or succinate buffers ($^{S}_{W}$pH∼ 6.11). The ionic strengths of all the buffers were fixed at 0.1 M by adding the necessary amount of potassium chloride when necessary. The compositions of the solutions at equilibrium were solved by using the extended Debye–Hückel theory, which estimates the activity coefficients of the ions in the bulk phase. The adsorption of the samples onto X-Bridge-C_{18} assumed a simple bi-Langmuir isotherm for the neutral species (or zwitterion) and a Langmuir isotherm for the ionizable species. Competition for adsorption between the neutral and the ionic species was neglected. The band profiles were calculated based on the equilibrium-dispersive model of chromatography. An excellent agreement was observed between the experimental and the calculated band profiles for all buffer solutions. This work validates the adsorption mechanism assumed in earlier work for neutral and ionizable species. It is consistent with the neutral species adsorbing weakly (due to dispersive interactions) onto and/or into the C_{18}-bonded layer (large number of sites) while the singly charged species adsorb strongly onto the few residual accessible silanol groups (due to charge–dipole interactions). Doubly charged species are not retained and are probably excluded from the pores of the hydrophobic stationary phase.

1. Introduction

Knowledge of the adsorption mechanism of acido-basic compounds is required for predicting their retention times and of their overloaded elution band profiles on RPLC columns. The chromatographic behavior of acido-basic compounds on silica-C_{18} columns under linear and/or their slightly overloaded conditions have been widely studied in the literature [1–6]. Yet, a consistent adsorption mechanism of acido-basic compounds on silica-C_{18} has not yet been established and many controversies regarding the adsorption of ionizable compounds are still lingering.

Usually, neutral compounds adsorb weakly on and into the C_{18}-bonded layer of RPLC phases, due to dispersive interactions. This was proven by frontal analysis results [7–9]. Two types of adsorption sites are usually encountered. Sites of the first type are usually located at the interface between the C_{18}-bonded layer and the bulk mobile phase and have a low adsorption energy. Sites of the second type have a higher adsorption energy (≃ +5 to 10 kJ/mol) and are located deeper inside the C_{18} layer. Statistically, the sample molecules spend some time between the C_{18} chains, as was confirmed by molecular mechanics [10].

Experiments showed that, for a given mobile phase composition, the ionized species is less retained and exhibits a stronger peak tailing than its conjugated neutral form [11,12]. The study of the adsorption isotherms of ionizable compounds and of their adsorption energy distributions showed the existence of few but strong adsorption sites which account for the strong peak tailing observed for ionic species [13]. Some authors suggested that peak tailing of ionized compounds is caused by electrostatic repulsion between the ions adsorbed onto a homogeneous adsorbent surface. This theory is justified and it certainly explains why the adsorption of electrolytes on electrodes decreases as observed in electrochemical studies and why the stability of colloids (e.g., made of surfactants) also decreases, as results of the repulsion between a charged surface (that of the electrode or the micelles) and the free ions of the same charge in the bulk phase surrounding the electrodes or micelles [14,15]. This approach was extended to the adsorption of ions in chromatography by Stahlberg [16], who

* Corresponding author at: Department of Chemistry, University of Tennessee, 552 Buehler Hall, Knoxville, TN, 37996-1600, USA. Tel.: +1 865 974 0733; fax: +1 865 974 2667.
E-mail address: guiochon@utk.edu (G. Guiochon).

0021-9673/$ – see front matter © 2009 Elsevier B.V. All rights reserved.
doi:10.1016/j.chroma.2009.07.064

proposed its use to account for the progressive decrease in the retention time of peaks and their enhanced tailing with increasing amount injected. This repulsion model has generally been accepted by the chromatographic community as a suitable adsorption model of ion behavior in chromatography. Yet, the microscopic description of a solid, homogenous, and impermeable adsorbent with immobilized charges on its surface in contact with an aqueous solution of organic solvents remains debatable when using standard silica-C_{18} stationary phase.

This model of electrostatic repulsion on a homogenous surface cannot explain, however, why, in the same time, the retention of ionized compounds would decrease and their peak tailing increase more significantly than those of their neutral conjugated species in the same eluent. There is a double contradiction here. (1) Electrostatic attractions being stronger than polar attraction forces, the ionic species should be more strongly adsorbed than the neutral forms. (2) When retention decreases on a homogeneous adsorbent, it is because the adsorption–desorption equilibrium constant decreases, which should necessarily result in a reduced peak tailing because, at constant sample size, the surface coverage decreases. Instead, the opposite is systematically observed. These contradictions can be alleviated if the energy of adsorption of the ions is larger but their adsorption sites are fewer than those of the conjugated neutral species, e.g. if the ionic and neutral compounds do not adsorb onto the same adsorption sites. The validity of this assumption was confirmed by the values measured for the adsorption energy distribution of ions and neutral conjugated forms that were determined in RPLC [9,13]. These results demonstrate the existence of few but very energetic adsorption sites for ions and of numerous but low adsorption energy sites for neutral compounds, the latter sites seeming unable to interact with ions.

Accordingly, a consistent thermodynamic adsorption model involving the existence of few, selective and high-energy adsorption sites on which ionized compounds are strongly adsorbed was proposed (multi-Langmuir adsorption isotherm). This model was validated under challenging conditions, in which the use of a weakly buffered mobile phase allowed the concentration ratio of the neutral and ionized species to vary widely during the elution of a large size band [13]. Later, overloaded elution band profiles of aniline recorded under experimental conditions leading to anti-Langmuir profiles were successfully accounted for using this model and applying the Debye–Hückel theory for calculating the ion activity in the bulk phase [17]. It must be emphasized that the thermodynamic interpretation of data provides book-keeping records of energies but cannot shed any light on the true microscopic description of adsorption mechanisms. Our model merely provides the degree of heterogeneity of the adsorption mechanism onto the silica-C_{18} adsorbent, the difference between the different adsorption energies involved, and the saturation capacity on each type of adsorption sites. The adsorption mechanisms identified by their thermodynamic characteristics may or may not involve electrostatic interactions between the adsorbent and the solutes. Other methods of investigations are required to answer this question.

The first goal of the present work was to go one step farther, consider compounds having two acido-basic functions, hence two pK_as and validate the extension of our earlier conclusions to the adsorption behavior of compounds having multiple acid and/or basic functions in RPLC. The validation of our model could have important consequences since almost all peptides have several pK_a. So, our second goal was to develop the necessary tools to model and predict the overloaded band profiles of complex acido-basic compounds such as small peptides [18], which is of paramount importance for their purification in the pharmaceutical industry. Compounds with two pK_a exist as three different conjugated species in equilibrium. Accordingly, we studied the overloaded band profiles of phthalic acid (${}^{W}_{W}$pKa,1 = 2.17 and ${}^{W}_{W}$pKa,2 = 4.82) and nicotinic acid (${}^{W}_{W}$pKa,1 = 2.89 and ${}^{W}_{W}$pKa,2 = 5.51) by using buffer solutions at ${}^{S}_{W}$pH between 1.35 and 7.32, prepared in a water-rich mixture (90/10 water/methanol, v/v). The molar fractions of each species in the mobile phase was determined by solving the thermodynamics problem and applying the general Debye–Hückel theory to account for the non-ideal behavior of the bulk mobile phase. Finally, we assumed a bi-Langmuir adsorption model for the neutral species, a Langmuir model for the conjugated ionic species, and no competition between them. The degree of agreement between the recorded and the calculated band profiles will be discussed and a physical description of the adsorption mechanism of complex acido-basic compounds with two pK_a proposed.

2. Theory

This section explains first how the composition and the ${}^{S}_{W}$pHs of the bulk mobile phase is calculated for all the buffer and sample concentrations used in the experiments. Then it describes the model of chromatography used to calculate the overloaded band profiles of phenol, phthalic acid, and nicotinic acid.

2.1. Solution thermodynamics

In this work, we systematically used aqueous solutions of methanol (10% methanol, v/v) as the eluent, at an ionic strength, I, as close as possible to 0.1 M for all the buffers.

In methanol–water solutions, protons are exchanged between water and methanol molecules (forming the H_3O^+ and $CH_3OH_2^+$ species). An eluent molecule can also lose one proton to form either the hydroxide (OH^-) or the methanolate (CH_3O^-) anion. The autoprotolysis constant of the binary eluent is defined as the product of the activities of the protonated forms of the eluent molecules and their associated anions. At room temperature, an aqueous mixture containing 10% methanol (v/v) has an autoprotolysis constant $K^S_{ap} = 10^{-14.03}$, a value very close to that of pure water ($K^W_{ap} = 10^{-14}$ [19]). In this work, we assume that the activity coefficients of H_3O^+ and $CH_3OH_2^+$ on the one hand and those of OH^- and CH_3O^- on the other are equal (i.e., $\gamma_{H_3O^+} = \gamma_{CH_3OH_2^+}$ and $\gamma_{OH^-} = \gamma_{CH_3O^-}$), then:

$$K^S_{ap} = a_{H^+}a_{O^-} = \gamma_{H_3O^+}\gamma_{OH^-}[H^+][O^-] \quad (1)$$

The activity coefficients of the ions in solution, γ_i, are estimated using the classical extended Debye–Hückel equation, which is usually valid for ionic strengths in the range of 10–100 mM [19]:

$$\log \gamma_i = -\frac{Az_i^2\sqrt{I}}{1 + Ba_i\sqrt{I}} \quad (2)$$

where z_i is the charge of the ion, A and B are two parameters that depend on the temperature and on the dielectric constant, ϵ, of the solvent, a_i is the effective solvated diameter of the ion, and I is the ionic strength of the solution. A and B are written [19,20]:

$$A = \frac{1.8246 \times 10^6}{(\epsilon T)^{3/2}} \quad (3)$$

$$B = \frac{50.29}{(\epsilon T)^{1/2}} \quad (4)$$

In a methanol–water solution containing 10% methanol (v/v), we have $\epsilon = 76.4$ and at 298.15 K [21], $A = 0.539$ and $B = 0.335$. The effective solvated diameter, a_i, depends on the nature of the ion i. The diameters of all the ions present in the buffer solution used are listed in Table 1[20]. The ionic strength of the solution is given by the following summation over all the ions present in solution at

Table 1
Effective solvated diameter a_i of organic and inorganic ions in water.

Ion	Name	a_i [Å]
Cations		
H^+	Hydronium	9.0
Na^+	Sodium	4.0
K^+	Potassium	3.0
$(C_6H_5)CH_2{}^+NH_3CH\text{-}CONH\text{-}Ala$	$^+$Phe-Ala	7.0
Anions		
OH^-	Hydroxide	3.5
CH_3O^-	Methanolate	3.5
$H_2PO_4^-$	Phosphate I	4.0
HPO_4^{2-}	Phosphate II	4.0
Cl^-	Chloride	3.0
$HCOO^-$	Formate	3.5
CH_3COO^-	Acetate	4.5
HCO_3^-	Carbonate I	4.0
CO_3^{2-}	Carbonate II	4.5
$Phe\text{-}CONH\text{-}CHCH_3COO^-$	Phe-Ala$^-$	7.0

equilibrium:

$$I = \frac{1}{2}\sum_i z_i^2 c_i \quad (5)$$

where c_i is the molar concentration of the ion i in the solution.

The solution thermodynamics was solved using Excel (Solver Add-ins) in order to determine the equilibrium concentrations of all the species present in the solution, hence the ionic strength of the solution. The ${}_W^S pK_a$ values of all the buffers (formic acid, acetic acid, phosphoric acid, hydrogenphosphate, succinic acid, and succinate) were directly taken from the literature [22,19]. The two pK_a values of nicotinic and phthalic acids were taken in pure water (${}_W^W pKa$) from [23,24]. They are listed in Table 2. The procedure followed to solve this problem is given elsewhere [11,12,17]. The equations include the thermodynamic equilibria (eluent autoprotolysis, buffer and sample acido-basic equilibria), the mass conservation of the buffer and the injected samples, and electroneutrality. Using an initial guess, the Excell program finds the unique [H^+] concentrations which satisfy the condition of electroneutrality of the solution. If the resulting ionic strength is different than the initial guess, this new ionic strength is taken as the new guess and the problem solved again until the calculated ionic strength converges to the initial guess.

2.2. Calculation of chromatographic band profiles

The overloaded band profiles of the acido-basic compounds were calculated using the equilibrium-dispersive model (ED) of chromatography [25]. This model assumes instantaneous equilibrium between the mobile and the stationary phases and a finite column efficiency characterized by an apparent axial dispersion coefficient, D_a. This coefficient accounts for the band broadening contributions of both the axial dispersive phenomena (molecular and eddy diffusion) and the finite mass transfer kinetics between the two phases in the column. The axial dispersion coefficient is:

$$D_a = \frac{uL}{2N} \quad (6)$$

where u is the mobile phase linear velocity, L the column length, and N the number of theoretical plates or apparent efficiency of the column measured under linear conditions, i.e., with samples that are so small that the column efficiency is independent of the sample size. In this model, the mass balance equation for a single component is written

$$\frac{\partial C_T}{\partial t} + u\frac{\partial C_T}{\partial z} + F\frac{\partial q_T}{\partial t} - D_a\frac{\partial^2 C_T}{\partial z^2} = 0 \quad (7)$$

where q_T and C_T are the total stationary phase and the total mobile phase concentrations of the acido-basic compound at equilibrium (i.e., are the sums of the concentrations of the conjugated acidic and basic species), respectively, t is the time, z the distance along the column, and $F = (1-\epsilon_t)/\epsilon_t$ is the phase ratio, with ϵ_t the total column porosity. q_T is related to C_T through the isotherm equation, $q_T = f(C_T)$. The adsorption isotherm considered in this work will be presented later in the result and discussion section.

2.2.1. Initial and boundary conditions for the ED model

At $t = 0$ (before injection), the concentrations of the solute and the adsorbate in the column are uniformly equal to zero and the stationary phase is in equilibrium with the pure mobile phase. The boundary conditions used are the classical Danckwerts-type boundary conditions [25,26] at the inlet and outlet of the column.

At $z = 0$ (at the column inlet), the inlet concentration profile was determined by replacing the column by a union connector and recording the corresponding extra-column band profiles. This experimental profile was used as the inlet concentration profile in the numerical solutions of the ED model.

2.2.2. Numerical solutions of the ED model

The ED model was solved using a computer program based on an implementation of the method of orthogonal collocation on finite elements (OCFE) [27–29]. The number of subdomains was fixed as high as 300 in order to avoid undesired oscillations in the calculated signals when either front or rear shocks are formed. The set of discretized ordinary differential equations was solved with the Adams–Moulton method, implemented in the VODE procedure. The relative and absolute errors of the numerical calculations were 1×10^{-6} and 1×10^{-8}, respectively.

Table 2
${}_W^S pKa$ of the buffers and samples in the mobile phase mixture (H_2O/MeOH,90/10,v/v) $T = 298$ K.

Buffers (number in Table 4)	${}_W^S pKa1$	${}_W^S pKa2$
Formate [a] (IV)	3.80	–
Acetate [a] (V and VI)	4.85	–
Phosphate [a] (II, III, and VIII)	2.30	7.40
Succinate [b] (VII)	4.39	5.84
Samples	**${}_W^W pKa1$**	**${}_W^W pKa2$**
o-Phthalic acid [c]	2.89	5.51
Nicotinic acid [d]	2.14	4.82

[a] ${}_W^S pKa$ estimated from Fig. 2 in Ref. [16].
[b] From Ref. [19].
[c] From Ref. [21].
[d] From Ref. [20].

3. Experimental

3.1. Chemicals

The mobile phase was a solution of methanol and water (10/90, v/v), both HPLC grade from Fisher Scientific (Fair Lawn, NJ, USA). The mobile phase was filtered before use on a surfactant-free cellulose acetate filter membrane, 0.2 μm pore size (Suwannee, GA, USA).

The compounds used in this work were phenol, phthalic acid (${}_W^W pKa,1 = 2.89$ and ${}_W^W pKa,2 = 5.51$), nicotinic acid (${}_W^W pKa,1 = 2.17$ and ${}_W^W pKa,2 = 4.82$), and sodium nicotinate (Fig. 1). Hydrochloric acid (37% HCl), phosphoric acid (85% H_3PO_4), potassium dihydrogenphosphate (KH_2PO_4), dipotassium hydrogenphosphate (K_2HPO_4), formic acid (98% HCOOH), sodium formate (NaHCOO), acetic acid (>99.5% CH_3COOH), sodium acetate ($NaCH_3COO$), succinic acid (99% $HOOC(CH_2)_2COOH$), disodium succinate ($Na_2OOC(CH_2)_2COO$), and potassium chloride (KCl) all from

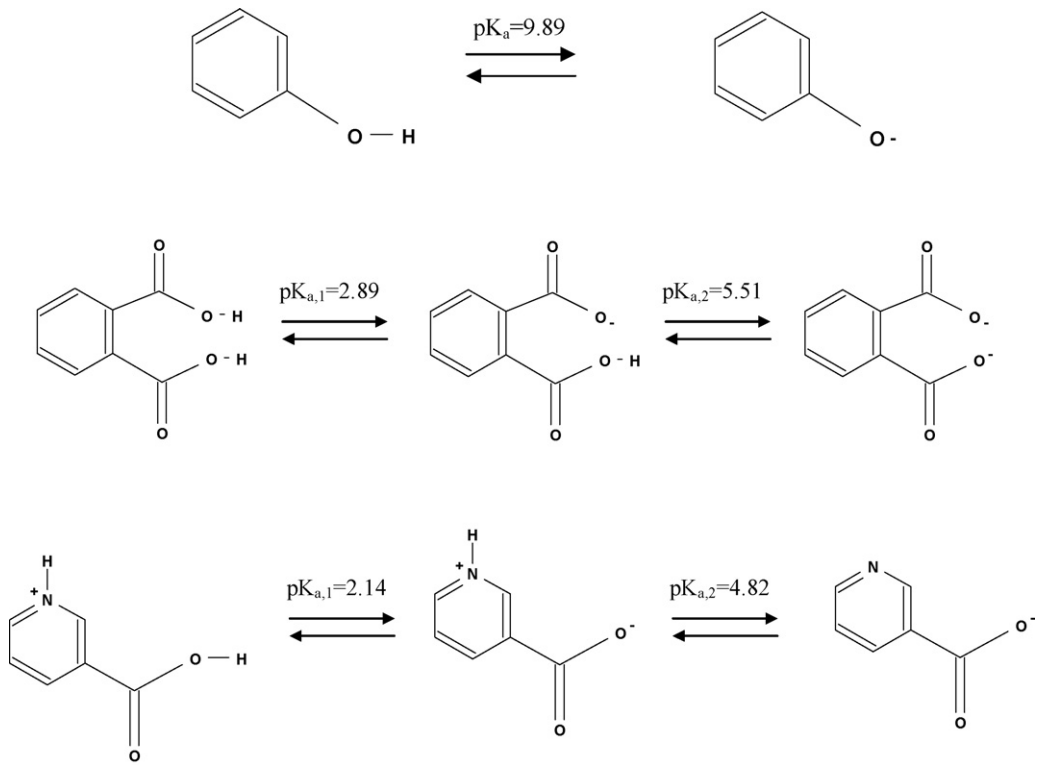

Fig. 1. Chemical structures and conjugated species of phenol, o-phthalic acid, and nicotinic acid used in this study. The pK_a values indicated are those in pure water (^W_WpKa).

Fisher Scientific, were used to prepare the buffer solutions (see Table 3 for the ^S_WpH of the buffers and their concentrations).

3.2. Materials

An Agilent 1090 liquid chromatograph was used to perform the measurements. This instrument includes a ternary solvent delivery system, an auto-sampler with a 250 μL sample loop, a diode-array UV detector (cell volume 1.7 μL, sampling rate 25 Hz), a column oven, and a data station running the HP data software. From the needle seat to the column inlet and from the column outlet to the detector cell, the total extra-column volume of the instrument is 45 μL, measured as the apparent hold-up volume of a zero-volume union connector in place of the column.

The chromatographic column (150 × 4.6 mm packed with X-Bridge-C_{18} particles, average size 3.5 μm, average pore size 136 Å, specific surface area 172 m^2/g, bonding density 16.95% C, 3.13 μmol/m^2) was a generous gift from Waters (Milford, MA, USA). The total porosity $\epsilon_t = 0.637$ of this column was estimated from pycnometric measurements (made using methanol and dichloromethane), giving a column hold-up volume of 1.588 mL [17]. The packing material was endcapped according to a proprietary process. Table 4 summarizes the manufacturer's data.

The ^S_WpHs of the prepared mobile phase were measured with an Accumet pH-meter (Fischer Scientific), calibrated in pure water with two standard aqueous solutions at pH=4.00 and 9.00. Table 3 lists all the results of the measurements. The measured ^S_WpHs are in very good agreement with the calculated ones. A substantial junction potential associated with the two most acidic buffers 1 and 2 could explain the larger than average pH differences between experiments and calculations.

3.3. Buffer and sample preparation

Eight buffer solutions (total volume 500 mL) were prepared by dissolving the appropriate amounts of the acid and its conjugated base (see columns 2 and 3 of Table 3) in order to obtain ^S_WpH values increasing regularly from 1.5 to 7.0 at a constant ionic strength of 0.1 M. Potassium chloride was added to hydrochloric acid in order to keep the ionic strength at 0.1 M for the lowest ^S_WpH value (1.37). All the measured ^S_WpH and the calculated ionic strengths of the buffers are listed in columns 5 and 8 of Table 3, respectively.

For each buffer solution, three 30 mM solutions of phthalic acid, nicotinic acid, and sodium nicotinate were prepared by dissolving 0.1246, 0.0923, and 0.1088 g, respectively, in a 25 mL volumetric glass. Accordingly, the largest sample concentrations of phthalic acid, nicotinic acid, and sodium nicotinate were 4.98, 3.69, and 4.35 g/L, respectively. It is important to note here that, at these moderate concentrations, the surface coverage of the adsorbent surface is smaller than 10%, so the contribution of the large number of weak adsorption sites at the interface between the C_{18} alkyl chains and the eluent to the non-linear behavior of the adsorption isotherm is negligible.

For each sample solution, a calibration curve $C = f(Abs)$ was experimentally determined by using different mixing ratios of the effluents of pumps A (neat buffer) and B (sample solution). The mixing ratios were 2, 5, 10, 20, 35, 50, 65, 80, and 100%. These calibration curves were necessary to transform the records of the UV-signals into total concentration profiles (sums of the concentrations of all species) profiles as a function of the elution time.

3.4. Injections

The injected samples were 5 and 50 μL of the 30 mM sample solution. The flow rate was set at 0.5 mL/min (inlet column pressure close to 125 bar) and the temperature was maintained at 295 ± 1 K by the lab air-conditioning system.

3.5. pH measurements

The details on the measurements of the buffer and sample solutions ^S_WpHs were given elsewhere [17]. "^S_WpH" means that the pH

Table 3
Preparation of the buffer solutions in a water/methanol (90/10, v/v) mixture. Ionic strength calculated for the neat buffer solutions and the sample solution containing 30 mM of dissolved phthalic acid, nicotinic acid, and sodium nicotinate. Comparison between the measured $^{S}_{W}$pHs (given in bold) and the calculated $^{S}_{W}$pHs.

Buffer number	Acid [M]	Base [M]	Supporting salt [M]	Ionic strength [M]		Buffer		30 mM o-phthalic acid sample		30 mM nicotinic acid sample		30 mM sodium nicotinate sample	
				Buffer	Samples	$^{S}_{W}$pH Theo.	$^{S}_{W}$pH Exp.	$^{S}_{W}$pH Theo.	$^{S}_{W}$pH Exp.	$^{S}_{W}$pH Theo.	$^{S}_{W}$pH Exp.	$^{S}_{W}$pH Theo.	$^{S}_{W}$pH Exp.
I	HCl **0.036**	KH_2PO_4	KCl **0.056**	0.092	0.093 0.092 0.093	1.53	**1.37**	1.52	**1.35**	1.88	**1.71**	2.88	**2.93**
II	H_3PO_4**0.103**	K_2HPO_4**0.093**	None	0.102	0.103 0.114 0.138	2.11	**2.01**	2.07	**1.98**	2.21	**2.14**	2.43	**2.37**
III	H_3PO_4**0.018**	K_2HPO_4**0.099**	None	0.101	0.102 0.104 0.129	2.85	**2.85**	2.59	**2.58**	2.96	**2.95**	4.42	**4.44**
IV	HCOOH **0.100**	HCOONa **0.100**	None	0.100	0.101 0.101 0.131	3.63	**3.61**	3.42	**3.40**	3.63	**3.60**	3.84	**3.83**
V	CH_3COOH **0.170**	CH_3COONa 0.100	None	0.100	0.102 0.100 0.130	4.47	**4.47**	4.23	**4.21**	4.42	**4.38**	4.57	**4.58**
VI	CH_3COOH **0.031**	CH_3COONa **0.100**	None	0.100	0.107 0.100 0.130	5.22	**5.25**	4.68	**4.70**	4.97	**4.94**	5.40	**5.38**
VII	Succinic acid **0.004**	Disodium succinate **0.034**	None	0.098	0.077 0.082 0.135	6.09	**6.11**	4.70	**4.69**	5.29	**5.16**	6.87	**6.71**
VIII	KH_2PO_4**0.020**	K_2HPO_4**0.030**	None	0.110	0.082 0.105 –	7.32	**7.32**	4.08 6.98 [a]	**4.18** **6.93**[a]	–	–	–	–

[a] pH values calculated and measured for a 0.005 M solution of phthalic acid.

Table 4
Physico-chemical properties of the column used in this work according to the manufacturer.

Neat silica	X-Bridge 3.5 μm
Particle size [μm]	3.5
Pore diameter [Å]	136
Surface area [m^2/g]	172
Bonded phase	X-Bridge-$C_1$8
Total carbon [%]	16.95
Surface coverage [μmol/m^2]	3.13
Endcapping	Yes
Packed column	
Serial number	128B3812113683
Dimension (mm × mm)	4.6 ×150
Total porosity [a]	0.637

[a] Measured by pycnometry (CH_3OH/CH_2Cl_2) at 295 K.

of the solution was directly measured in the solution (S) after the electrode was calibrated in pure water (W).

4. Results and discussion

4.1. Saturation capacity of the X-bridge-C_{18} column

In order to determine the best adsorption isotherm parameters of o-phthalic and nicotinic acid by the inverse method of chromatography (using experimental overloaded band profiles, 50 μL injection volume), it is important to estimate first the saturation capacity $q_{S,1}$ of the weakest type of adsorption sites, which corresponds to an adsorbed monolayer onto the X-bridge C_{18} adsorbent. The plausibility of the best saturation capacity $q_{S,1}$ given by the fitting procedure compared to realistic values supports the adsorption model chosen.

The specific volume of the unbonded hybrid organic/inorganic BEH material is 0.66 cm^3/g. The density of the BEH skeleton is 2.02 g/cm^3. The porosity of the unbonded particles is then $\epsilon_p^0 = 0.57$. Assuming an external porosity of the packed bed of $\epsilon_e = 0.38$, the volume of the column tube being $V_C = 2.49\ cm^3$, the volume of neat BEH adsorbent inside the column, V_{BEH}, is:

$$V_{BEH} = (1-\epsilon_e)(1-\epsilon_p^0)V_C = 0.67\ cm^3 \quad (8)$$

The mass of unbonded BEH adsorbent is then 0.67 cm^3×2.02 g/cm^3=1.35 g and its surface area is $S_{BEH} = 1.35\ g \times 172\ m^2/g = 232\ m^2$. The actual surface area available onto the BEH-C_{18} packing material is smaller, due to the thickness of the C_{18}-bonded layer covering the wall of the mesopores. The total porosity of the column is $V_0 = \epsilon_t \times V_C = 1.59\ cm^3$. Hence, the volume of the hydrophobic bonded layer is equal to $V_{C_{18}} = V_C - V_0 - V_{BEH} = 2.49 - 1.59 - 0.67 = 0.23\ cm^3$. The average thickness of the layer is $\tau_{C_{18}} = V_{C_{18}}/S_{BEH} = 10$ Å. Assuming that the mesopores are spherical with an average mesopore diameter of the unbonded material ($D_p = 136$ Å), the corrected surface area available onto the BEH-C_{18} adsorbent is

$$S_{BEH-C_{18}} = S_{BEH}\left(1 - \frac{\tau_{C_{18}}}{D_p}\right)^2 = 199\ m^2 \quad (9)$$

Consider the formation of a monolayer of phenol, phthalic acid, or nicotinic acid. Their density ρ_i (molecular weight M_i) at 298 K are 1.07 g/cm^3 (M = 94.1 g/mol), 1.59 g/cm^3 (M = 166.14 g/mol), and 1.47 g/cm^3 (M = 123.11 g/mol). Assume the molecules of these compounds to be hard spheres adsorbed on the surface. The average van der Waals diameter D_i of these molecules are

$$D_i = \sqrt[3]{\frac{6M_i}{\pi\rho_i N_{av}}} \quad (10)$$

where N_{av} is Avogadro number (6.02×10^{23} mol^{-1}). The molecular sizes of phenol, phthalic acid, and nicotinic acid are 6.5 , 6.9, and 6.4 Å, respectively. Assuming a hexagonal lattice, simple geometric considerations give the maximum number of moles of hard spheres of diameter D_i, $n_{S,i}$, that can be packed as a dense monolayer onto a surface $S_{BEH-C_{18}}$:

$$n_{S,i} = \frac{1}{\sqrt{3}N_{av}}\frac{S_{BEH-C_{18}}}{D_i^2} \quad (11)$$

The saturation capacity of compound i expressed in gram per unit volume of adsorbent is:

$$q_{S,i} = \frac{n_{S,i}M_i}{(1-\epsilon_t)V_C} \quad (12)$$

This approximation gives estimates of the saturation capacities of phenol, o-phthalic acid, and nicotinic acid as 47, 74, and 63 g/L, respectively. Obviously, estimates of the saturation capacity of the stronger type of adsorption sites, $q_{S,2}$, located deeper within the C_{18}-bonded layer [9,10], cannot be derived from such simple geometrical considerations. It will have to be directly estimated using the inverse method and minimizing the difference between the calculated and experimental overloaded band profiles.

4.2. Determination of estimates of the isotherm parameters by the inverse method

In the next sections of this work, the isotherm parameters of phenol, o-phthalic and nicotinic acid will be estimated using the inverse method of chromatography. The principle, accuracy, and precision of this method were discussed previously [30]. Basically, the inverse method permits an accurate determination of the adsorption isotherm parameters on the sites of type i only if these adsorption sites are well populated when the most overloaded band profile is recorded.

The validity of the saturation capacity $q_{S,1}$ was checked for phenol ($q_{S,1}$ = 47 g/L) by injecting 150 μL of a 60 g/L solution in the mobile phase. The best set of parameters is given in Table 5. The excellent agreement between the experimental (empty stars) and the calculated (solid red line) band profiles is illustrated in Fig. 2. The adsorption isotherm of phenol from water–methanol solutions to C_{18} surfaces is known to be a bi-Langmuir isotherm [9]. With a water-rich eluent as the one used in this work, the saturation capacities on the weak and strong types of adsorption sites are comparable, as shown in a gradient elution study [31]. Frontal analysis experiments have shown that the saturation capacities of phenol, $q_{S,1}$ and $q_{S,2}$, were close to 100 g/L on a 100 ÅKromasil-C_{18} adsorbent [32]. On the 136 Å X-Bridge-C_{18} column, the best estimate for the parameter $q_{S,1}$ on the weak type of adsorption sites is 50.0 g/L (a value in very close agreement with the estimate made earlier for the monolayer capacity, 47 g/L) while $q_{S,2}$ on the strong type of adsorption sites is 44.7 g/L.

Because the maximum concentrations of o-phthalic and nicotinic acid injected are significantly less than 60 g/L (30 mM, e.g. ≃ 5 g/L), the inverse method cannot provide precise estimates of the saturation capacity $q_{S,1}$ of these compounds on the weak adsorption sites because these sites are not significantly overloaded at the column inlet ($b_1C_{inlet}/(1+b_1C_{inlet}) < 10\%$). On the other hand, the inverse method will provide precise estimates of the isotherm parameters $q_{S,2}$ and b_2 since the high-energy adsorption sites are strongly populated at the column inlet ($b_2C_{inlet}/(1+b_2C_{inlet}) > 75\%$). As a result, we will assume that the estimates of $q_{S,1}$ for

Table 5
Best isotherm parameters of phenol, phthalic acid, nicotinic acid, and their conjugated species onto the X-bridge C18 column. The relative error made on the estimated parameters was always smaller than 15%.

Species i	Buffer	N	$q_{S,1,0}$ [g/L]	$b_{1,0}$ [L/g]	$q_{S,2,0}$ [g/L]	$b_{2,0}$ [L/g]	$q_{S,I}$ [g/L]	b_I [L/g]
Phenol	No buffer	2,000	50	0.059	45	0.37	–	–
Phthalic acid	I	5,000	74	0.019	41	0.64	5.7	0 [a]
Phthalate I	V	2,500	74	0 [a]	41	0 [a]	5.7	0.63
Phthalate II	VIII	13,000	74	0 [a]	41	0 [a]	5.7	0 [b]
Nicotinium	I	12,500	63	0 [a]	56	0 [a]	1.9	0.048
Nicotinic acid	IV	8,500	63	0.0012	56	0.0076	1.9	0 [a]
Nicotinate	VII	2,500	63	0 [a]	56	0 [a]	1.9	0.32

[a] These isotherm parameters were set to zero based on the assumption of a non-competitive adsorption mechanism between the neutral and the ionic species.
[b] This isotherm parameter cannot be measured based on the quasi-zero retention of the doubly charged phthalate II anion.

o-phthalic and nicotinic acid from Eq. (12) are correct. Note that, because the equilibrium constant b_1 is about one order of magnitude smaller than the equilibrium constant b_2, the possible error made on the parameter $q_{S,1}$ will not affect much the estimates of the isotherm parameters $q_{S,2}$ and b_2 on the strong adsorption sites, which control the retention (85%) and the shape (peak tailing) of the band profiles of o-phthalic acid under the moderate overloading conditions performed in this work.

4.3. Determination of the general adsorption isotherm of phthalic acid

O-phthalic acid has two ${}^{W}_{W}$pKa, at 2.89 and 5.51. Three different species can exist in the solution, depending on the mobile phase pH, the neutral species o-phthalic acid, the singly charged mono-anion phthalate I, and the doubly charged di-anion phthalate II. The primary goal of this study is to determine the adsorption isotherm parameters of each one of these species in solutions having appropriate pH values. According to the data in Table 3, buffer I, buffer V, and buffer VIII will be chosen to estimate the isotherm parameters of o-phthalic acid, phthalate I, and phthalate II, respectively.

4.3.1. Isotherm parameters of neutral o-phthalic acid

The general adsorption isotherms of neutral compounds in RPLC involves adsorption sites whose surface area corresponds to the surface of contact between the C_{18}-bonded phase and the stagnant eluent inside the particles' mesopores. The adsorption energy of these sites was found to be much smaller than that of the few active adsorption sites onto which their conjugated ionized species are specifically adsorbed [9,13]. Such an adsorption model was recently validated by the excellent agreement between the band profiles of acido-basic compound having one pK_a (anilinium/aniline) that were calculated with our model and those that were recorded on modern commercial RPLC columns [17].

The adsorption isotherm of o-phthalic acid was assumed to be similar to that of phenol, e.g. to be a bi-Langmuir adsorption isotherm. This assumption is reasonable because both compounds have similar structures, with a hydrophobic phenyl group attached to a polar group. We further assume that the ionized forms of o-phthalic acid are adsorbed on different types of active sites and do not compete with the neutral species for adsorption due to the negligible adsorption constant of anions on the hydrophobic C_{18} surface.

The ${}^{S}_{W}$pH of the (HCl, KCl) buffer I was found equal to 1.37. When dissolving 30 mM of o-phthalic acid in it, the ${}^{S}_{W}$pH of the sample solution became 1.35. The concentration of the doubly charged phthalate anion was neglected because its molar fraction is less than 0.001% at this acidic pH. The molar compositions were calculated by solving the set of thermodynamic equations as a function of the total concentration C_T. Then, the general adsorption isotherm becomes

$$q_T = q_{S,1,0}\frac{b_{1,0}\alpha_0 C_T}{1+b_{1,0}\alpha_0 C_T} + q_{S,2,0}\frac{b_{2,0}\alpha_0 C_T}{1+b_{2,0}\alpha_0 C_T} + q_{S,I}\frac{b_I\alpha_I C_T + b_{II}\alpha_{II} C_T}{1+b_I\alpha_I C_T + b_{II}\alpha_{II} C_T} \quad (13)$$

where α_0, α_I, and α_{II} are the molar fractions of phthalic acid, phthalate I, and phthalate II, respectively, $q_{S,1,0}$, $q_{S,2,0}$, $b_{1,0}$, and $b_{2,0}$ are the saturation capacities and the equilibrium constants of phthalic acid on sites 1 and 2, and $q_{S,I}$, b_I, and b_{II} are the saturation capacities of the adsorption sites specific to ionic species and the equilibrium constants of the singly and doubly charged phthalate anions. Fig. 3A shows the molar fraction of each species as a function of the total concentration of phthalic acid dissolved in buffer I.

Fig. 4A compares the experimental (empty stars) and the best calculated (solid red line) band profiles. The best isotherm parameters found were $b_{1,0} = 0.0195$ L/g, $q_{S,2,0} = 41.1$ g/L, and $b_{2,0} = 0.64$ L/g (with $q_{S,1,0} = 73.6$ g/L, according to the estimate based on Eq. (12)). Because the molecule of o-phthalic acid is larger than that of phenol, the ratio $q_{S,2}/q_{S,1}$ increases from 1.12 to 1.79, due to a larger exclusion of phthalic acid from the internal pore space hindered by the C_{18}-bonded layer [7,8].

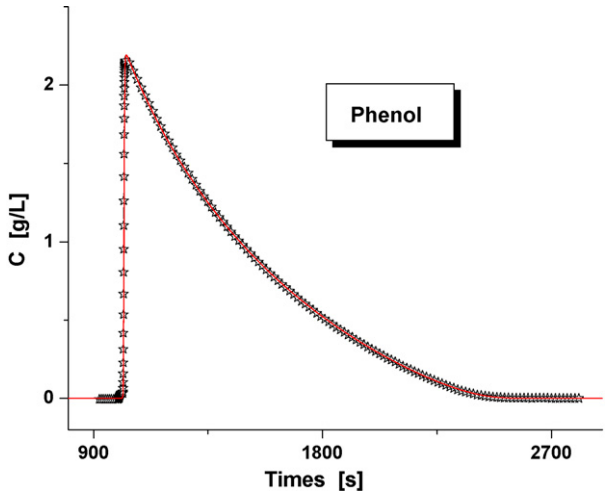

Fig. 2. Best agreement between the experimental (empty stars) and calculated (solid red line) band profiles of phenol. Sample: 150 μL of a 60 g/L solution of phenol dissolved in a methanol–water mixture (10/90, v/v). $T = 295$ K. Flow rate 0.50 mL/min. The best adsorption isotherm parameters of phenol are given in Table 5. (For interpretation of the references to color in the figure caption, the reader is referred to the web version of the article.)

4.3.2. Phthalate I species

The ${}^{S}_{W}$pH of the acetate buffer V is equal to 4.47. After dissolution of 30 mM of o-phthalic acid, the ${}^{S}_{W}$pH drops to 4.21. At such a pH, the calculation of the molar fractions showed that phthalic acid is

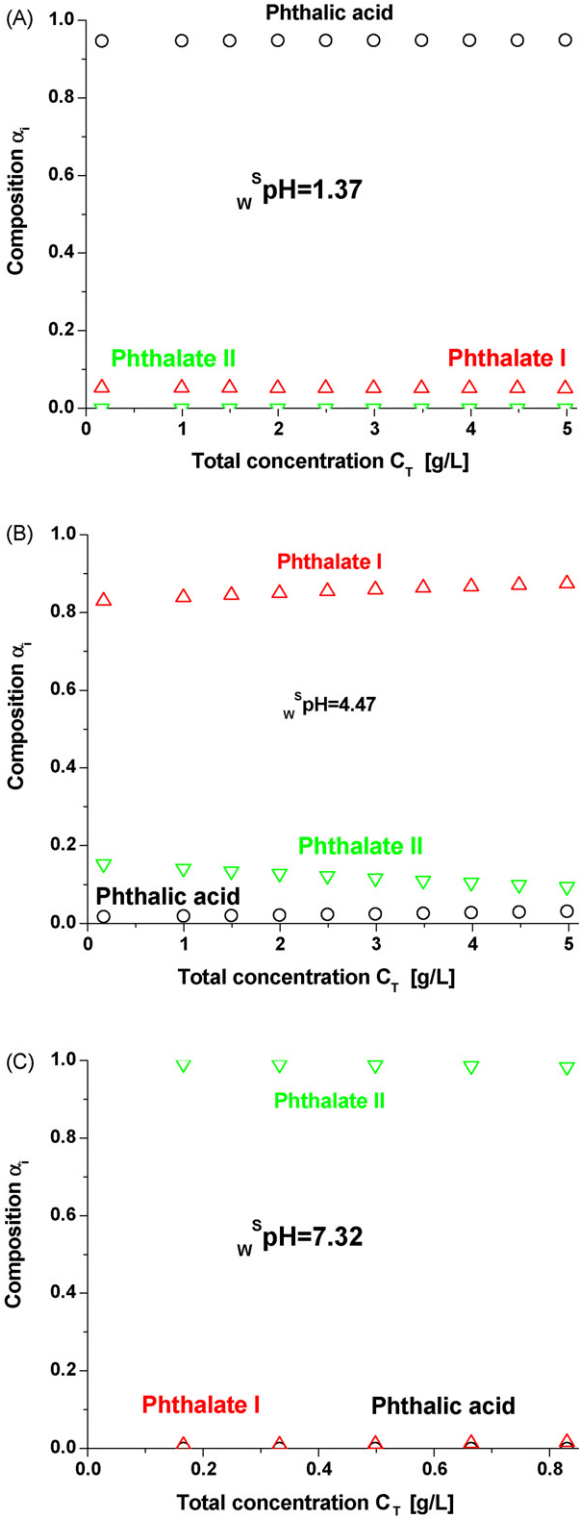

Fig. 3. Calculated molar fractions of the different phthalic acid species as functions of the total concentration C_T of phthalic acid dissolved into three different buffer solutions (A), (B), and (C). Note the predominance of phthalic acid, of the singly charged phthalate anion, and of the doubly charged phthalate anion at buffer $^{S}_{W}$pH 1.37, 4.47, and 7.32, respectively.

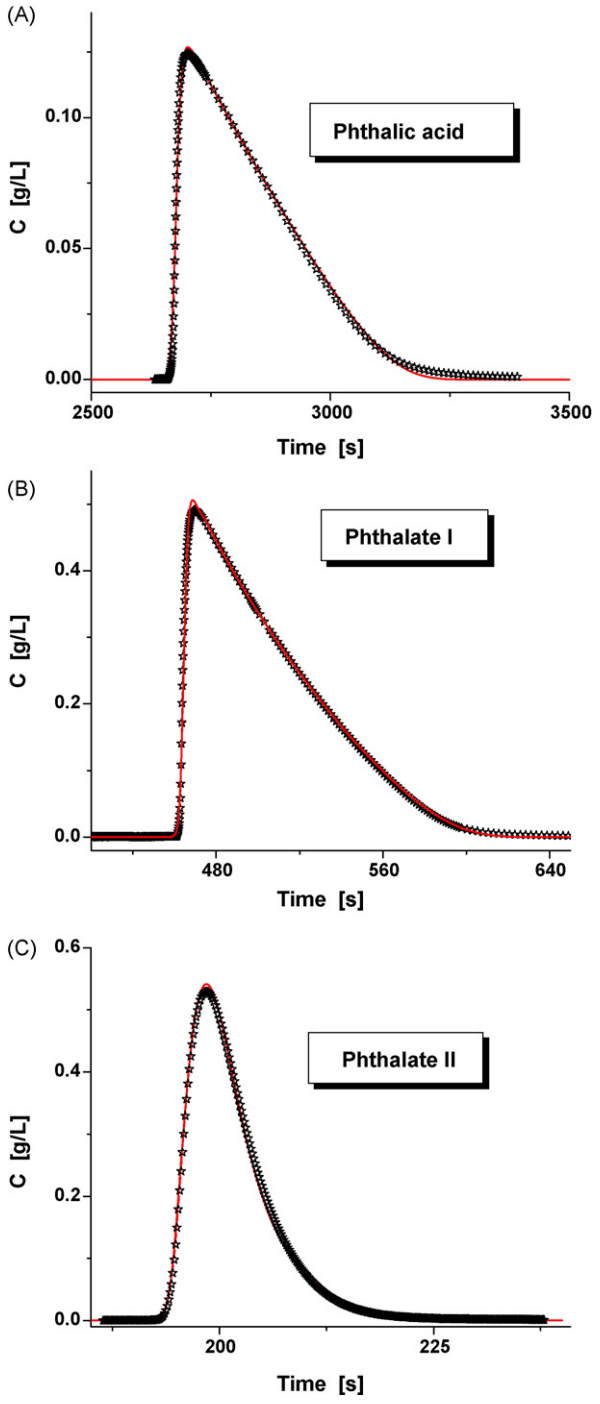

Fig. 4. Experimental (empty stars) and calculated (solid red line) band profiles of phthalic acid at three different buffer $^{S}_{W}$pH 1.37 (A), 4.47 (B), and 7.32 (C) . Sample: in (A) and (B), injection of 50 μL of a 30 mM solution of pthalic acid dissolved in the buffer solutions; in (C), injection of 50 μL of a 5 mM solution of phthalic acid. T = 295 K. Flow rate 0.50 mL/min. The best adsorption isotherm parameters of phthalic acid, phthalate I, and phthalate II anions are given in Table 5. (For interpretation of the references to color in the figure caption, the reader is referred to the web version of the article.)

not quantitatively dissociated into the phthalate I anion ($\simeq$ 97.5% only). Because the retention of the neutral o-phthalic acid species is much larger than that of the charged species, even a molar fraction as small as 2.5% can affect the overall retention of phthalic acid at $^{S}_{W}$pH = 4.47. The variations of the molar composition of the bulk mixture as a function of the total concentration of phthalic acid dissolved is shown in Fig. 3B. Fig. 4B compares the best calculated and experimental band profiles obtained with the same isotherm parameters reported above and with $q_{S,I}$ = 5.7 g/L and b_I = 0.63 L/g. We note that the adsorption energy $\epsilon_I = RT \ln b_I/b_0$ (b_0 is the pre-exponential factor which can be assumed independent of the type of adsorption sites [33]) of the monovalent anion on the adsorption sites I is equivalent to that of the neutral acidic species

onto the sites of type 2 ($\epsilon_{2,0} = RT \ln b_{2,0}/b_0$) but the corresponding number of accessible sites is smaller (a one to seven ratio). The sites of type 2 are located within the C_{18} chain layer and the neutral species can easily diffuse from the tip of the C_{18} chains and have access to them. On the other hand, the charged species does not statistically occupy these sites or has a nearly negligible adsorption energy (this is one of our initial assumption that lead to the isotherm model Eq. (13), e.g. the non-competitive isotherm). The adsorption sites I accessible to the mono-anion phthalate I are probably located at the surface of the silica (on which the ionized compound can be strongly adsorbed) amidst the C_{18}-bonded chains. We observed in a previous report that the stronger the ionic strength, the larger the access to these sites and the smaller the adsorption constant. This is consistent with a possible ion–dipole interaction between unreacted silanol and the anion.

4.3.3. Phthalate II species

The ${}^{S}_{W}$pH of the phosphate buffer VIII is equal to 7.32. After dissolution of only 5 mM (and not 30 mM) of o-phthalic acid, the ${}^{S}_{W}$pH drops to 6.93. As a result, the molar fractions of the acid and

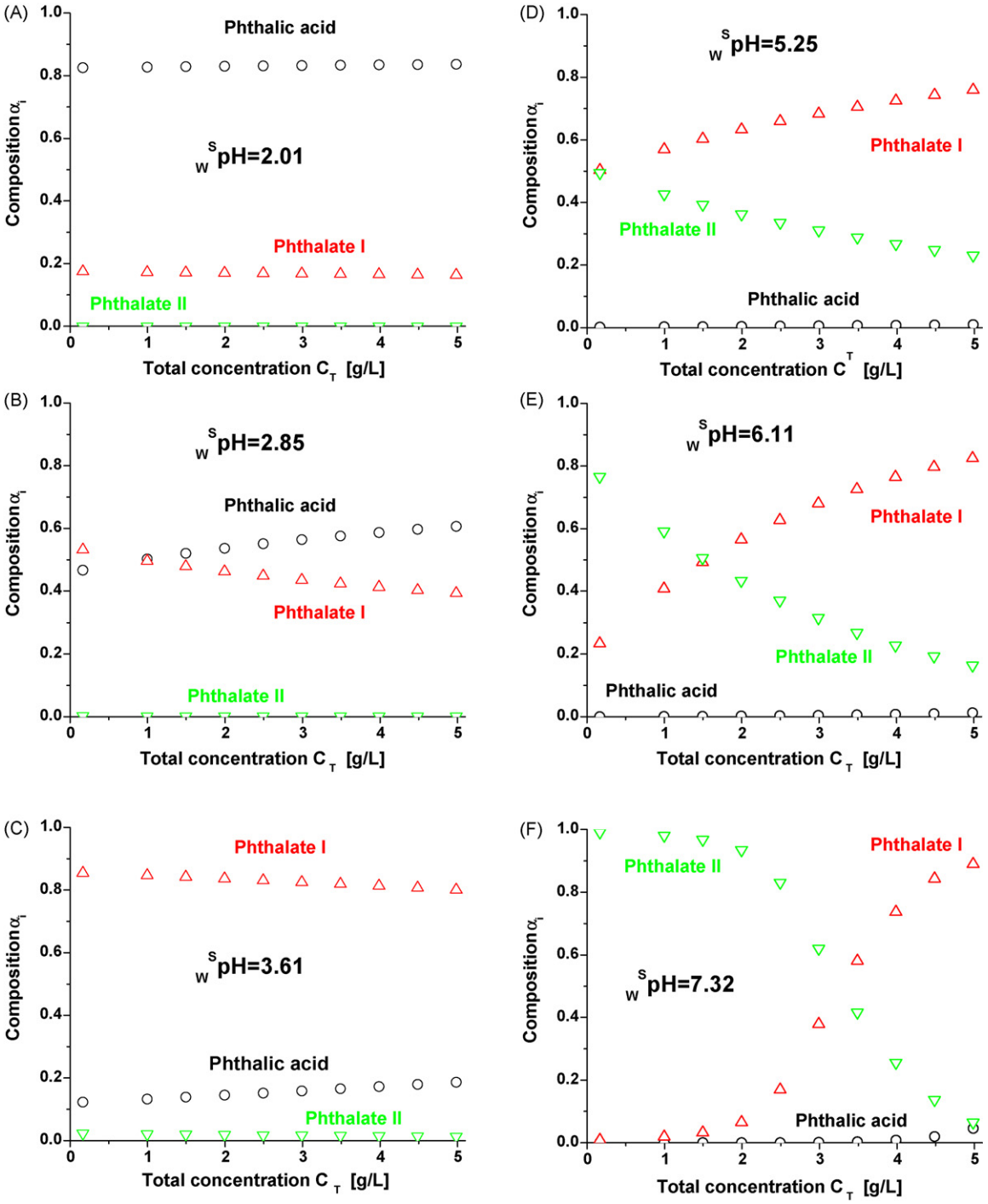

Fig. 5. Calculated molar fractions of the different phthalic acid species as functions of the total concentration C_T of phthalic acid dissolved into six different buffer solutions (A), (B), (C), (D), (E), and (F).

of the monovalent anion are negligible, 0.00005 and 1%, respectively (see Fig. 3C). The band is quasi-unretained and the doubly charged phthalate anion is practically not retained. The combination of the injection profile with the adsorption isotherm $q_T = 0$ gives an almost perfect fit to the experimental band profile, as shown in Fig. 4C.

4.3.4. Validation of the general adsorption isotherm model for phthalic acid

In the previous sections, we used three particular buffer solutions (I, V, and VIII) in order to determine the specific isotherm parameters of the three species of phthalic acid present in the solution. The neutral form adsorbs on two distinct types of sites (1 and 2), as phenol does. The monovalent phthalate anion adsorbs strongly on a few specific adsorption sites (sites of type I). Finally, the divalent phthalate anion is not retained on the column.

The best estimates of the parameters of the general adsorption isotherm were used to calculate the overloaded band profiles of samples of 30 mM phthalic acid dissolved in various buffer solutions at the constant ionic strength $I = 0.1$ M. Six different $^{S}_{W}$pH s were investigated, using the buffer solutions II, III, IV, VI, VII, and VIII. For each buffer solution, the molar fractions α_0, α_I, and α_{II} were calculated. Their plots as a function of the total concentration C_T of acid dissolved is given in Fig. 5A–F.

The agreement between the calculated (solid lines) and the experimental (dotted lines) band profiles is illustrated in Fig. 6A (all six overloaded band profiles are represented in the same graph to illustrate the change in retention), 6B and 6C (enlarged, better to assess the agreement between calculation and experiments). The isotherm parameters previously estimated are given in Table 5. We observe an excellent agreement at all $^{S}_{W}$pHs. The adjustable column efficiency N in the ED model was chosen so as to match the apex of the experimental and the calculated band profiles. Accordingly, the column efficiencies were 3000, 2500, 2000, 1500, 1500, 9000, and 13,500 when the $^{S}_{W}$pH s of the buffer solution were 2.01, 2.85, 3.61, 5.25, 6.11, and 7.32, respectively. The column efficiency is smaller when the monovalent phthalate anion is the predominant species than when phthalic acid is the main species in solution, despite the fact the retention of the neutral species is larger. Possibly, the stronger adsorption energy of the anion on the surface of the adsorbent leads to a slower adsorption–desorption kinetics. As the retention decreases more and more (the unretained bivalent phthalate anion becomes the main eluted species), the column efficiency increases strongly to a value expected for a 3.5 μm column. Assuming the HETP to be two and a half the particle diameter, e.g. 10.5 μm, the efficiency of the 15 cm long column would be about 150,000/10.5 ≃ 14000 plates.

4.4. Band profiles of a zwitterionic compound, nicotinic acid

In the preceding example, the net charge of the sample increased continuously with increasing pH of the solution (from 0 to −2). In this new case, we merely analyze the elution band profiles of nicotinic acid dissolved in the same buffer solutions as described in Table 3. The net charge of this compound is +1 at very acidic pHs, 0 at intermediate pH, and −1 at basic pHs.

Fig. 7A and B show the overloaded band profiles (injection of 50 μL of a 30 mM sample solution) of nicotinic acid and of sodium nicotinate, respectively. Whether the acid or the base are dissolved in the buffer solutions, similar overloaded band profiles are observed because solutions prepared from nicotinic acid or sodium nicotinate contain the same chemical species at each $^{W}_{S}$pH. However, we observed a slight difference at $^{S}_{W}$pH = 2.85 because the $^{W}_{S}$pH of the injected sample solutions are different (2.58 for nicotinic acid *versus* 4.44 for sodium nicotinate) so the ratios of the species concentrations are initially different in the injection loop.

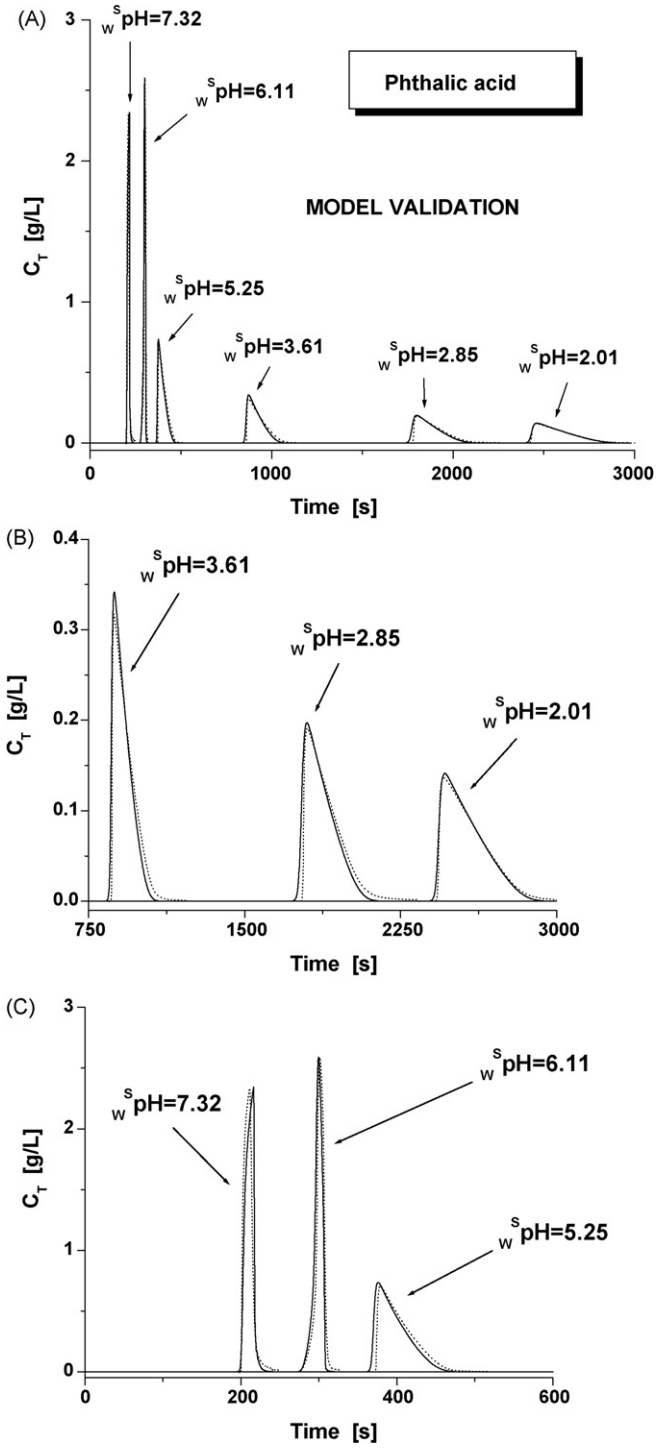

Fig. 6. (A) Comparison between the experimental (dashed lines) and the calculated (solid lines) elution band profiles of phthalic acid in six different mobile phase $^{S}_{W}$pHs. (B) Zoom in for the three most acidic $^{S}_{W}$pHs. (C) Zoom in for the less acidic $^{S}_{W}$pHs. Note the validity of the general adsorption isotherm model Eq. (13).

The retention of nicotinic acid on the X-bridge column is significantly less than that of phthalic acid in the mobile phase used.

The progressive evolution of the chromatograms with increasing mobile phase pH is interesting. At low $^{S}_{W}$pH (1.37 and 2.01), below or close to the first pK_a (2.17) of nicotinic acid, the cationic species, nicotinium, and the zwiterrionic species, nicotinic acid, are the only two forms of the sample present in solution. The peaks are fronting

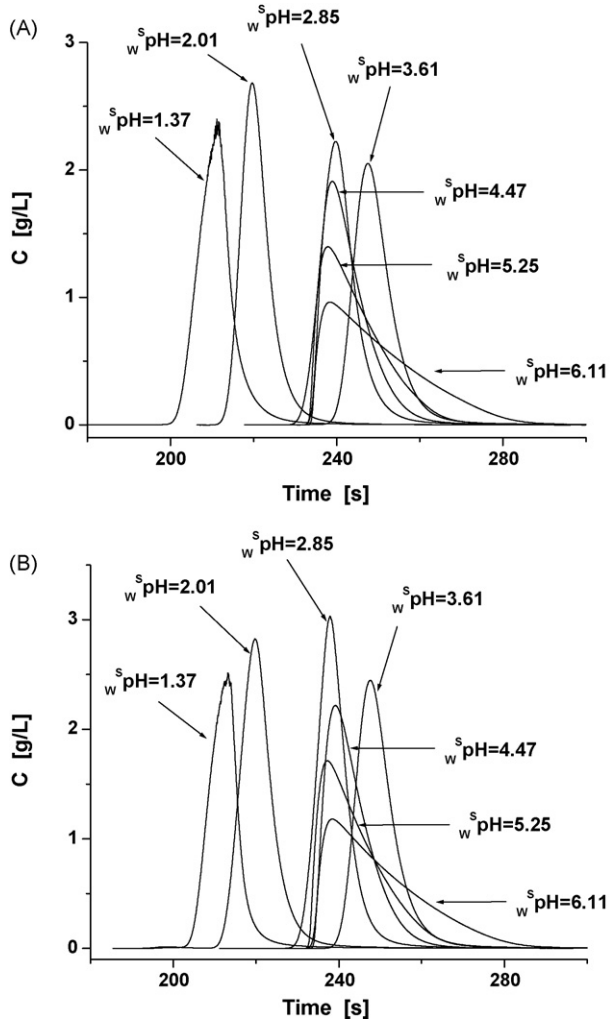

Fig. 7. Experimental band profiles of nicotinic acid (50 μL injection of a 30 mM sample solution, flow rate 0.50 mL/min) as a function of the mobile phase $^{S}_{W}$pH. (A) Sample introduced under its zwitterionic form (nicotinic acid). (B) Sample introduced under its anionic species (sodium nocotinate). Note the low retention factor of nicotinium cation and the large retention factor of nicotinate anion.

which suggests that nicotinium is hardly retained and nicotinic acid is more strongly retained. As the concentration increases, the ratio of nicotinium to nicotinic acid molecules decreases because the samples were injected as the zwiterrionic form or the negatively charged basic form. As the pH increases further (2.85 and 3.61), the peak becomes quasi-gaussian (the slight tailing is mostly due to the extra-column contribution). This is due to the zwiterrionic form being predominant in the bulk phase. Finally, when the mobile phase pH becomes close to or larger than the second pK_a (4.82) of nicotinic acid (4.47, 5.25, and 6.11), the negatively charged species nicotinate predominates in the bulk solution. In contrast to what was observed with the charged species nicotinium, nicotinate is the most retained species onto the X-bridge column. Most remarkably, the band profile tails significantly suggesting that a small number of strong adsorption sites are involved in the retention of nicotinate. In the next section, we determine the general adsorption isotherm of nicotinic acid for all buffer solutions, at the constant ionic strength $I = 0.1$ M.

4.4.1. Adsorption isotherm of the different forms of nicotinic acid

As observed above, the retention of nicotinic acid (neutral zwitterionic form) is rather weak. The simultaneous determination of all the isotherm parameters ($q_{S,1,0}$, $q_{S,2,0}$, $b_{1,0}$, and $b_{2,0}$) is impossible after the simple records of the band profiles shown in Fig. 7A and B. Initial guesses are required, based on the estimate of $q_{S,1}$ previously made from geometrical arguments ($q_{S,1,0} = 63.0$ g/L) and from the size of nicotinic acid relative to that of phenol (6.4 Å *versus* 6.5 Å). Because phenol and nicotinic acid have nearly the same size, we can reasonably assume that the ratio $q_{S,1,0}/q_{S,2,0}$ is the same for both compounds (1.12). So, $q_{S,2,0} = 56.2$ g/L for nicotinic acid. The equilibrium constants are then simply derived from the retention factor of nicotinic acid at $^{S}_{W}$pH = 3.61 (formate buffer IV) for which 90% of nicotinic acid remains under the zwitterionic form.

The retention time of infinitely dilute nicotinic acid at $^{S}_{W}$pH = 3.61 is 244 s. The hold-up time t_0 is 190 s. The phase ratio $F = (1 - \epsilon_p)/\epsilon_p$ is equal to 0.57. Accordingly, the Henry's constant of nicotinic acid is:

$$q_{S,1,0}b_{1,0} + q_{S,2,0}b_{2,0} = 63.0b_{1,0} + 56.2b_{2,0}$$
$$= \frac{1}{0.57}\left[\frac{244 - 190}{190}\right] = 0.50 \quad (14)$$

Let us assume that both equilibrium constants of nicotinic acid are the product of the equilibrium constants of phenol by the

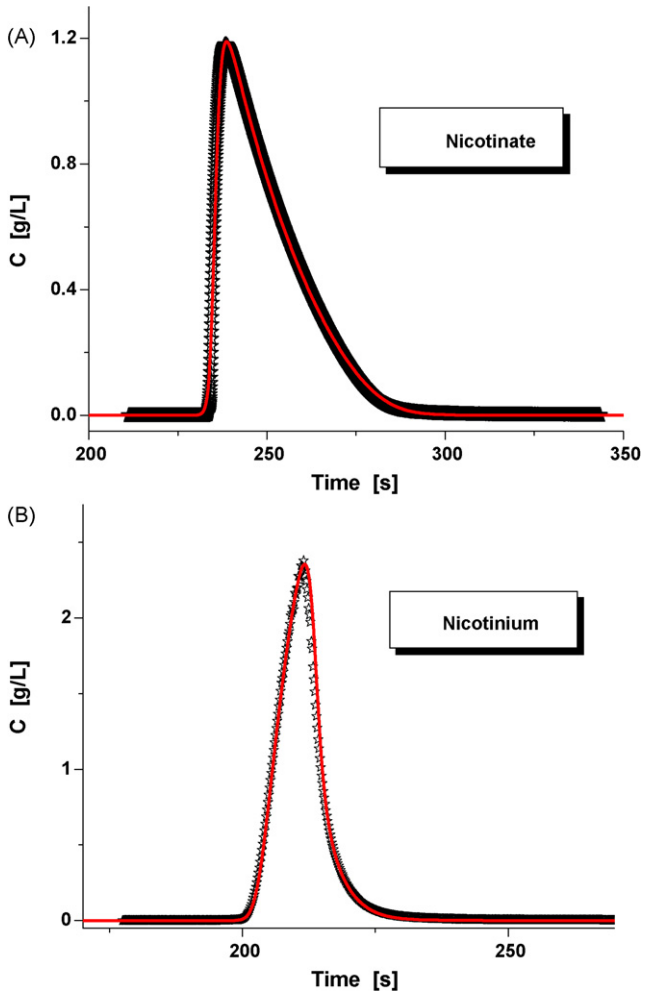

Fig. 8. Comparison between the experimental (empty stars) and calculated (solid red line) band profiles of nicotinic acid at two different buffer $^{S}_{W}$pH s 6.11 (A) and 1.37 (B). Injection of 50 μL of a 30 mM solution of nicotinic acid dissolved in the buffer solutions. $T = 295$ K. Flow rate 0.50 mL/min. The best adsorption isotherm parameters of the nicotinium cation and of the nicotinate anion are given in Table 5. (For interpretation of the references to color in the figure caption, the reader is referred to the web version of the article.)

same constant a. We found $a = 0.0204$, which means that the adsorption energy of nicotinic acid is 9.5 kJ/mol less than that of phenol. Accordingly, $b_1 = 0.0012$ L/g and $b_2 = 0.00755$ L/g. These small values explain why the overloaded band profiles of the zwiterrionic species are quasi-Gaussian since the surface coverage of the type sites 2 at the column inlet is less than 3%. These parameters will be used to determine the adsorption isotherm parameters of the nicotinate and nicotinium species. Again, we assume a non-competitive adsorption isotherm model of the ionic and neutral species and a competitive adsorption isotherm for the ionic species. We assumed that the active sites on which nicotinate and nicotinium can be adsorbed are the same. The general adsorption isotherm writes:

$$q_T = q_{S,1,0}\frac{b_{1,0}\alpha_0 C_T}{1 + b_{1,0}\alpha_0 C_T} + q_{S,2,0}\frac{b_{2,0}\alpha_0 C_T}{1 + b_{2,0}\alpha_0 C_T} + q_{S,I}\frac{b_{-I}\alpha_{-I}C_T + b_{+I}\alpha_{+I}C_T}{1 + b_{-I}\alpha_{-I}C_T + b_{+I}\alpha_{+I}C_T} \quad (15)$$

where α_0, α_{-I}, and α_{+I} are the calculated molar fractions of nicotinic acid, nicotinate anion, and nicotinium cation, respectively, $q_{S,I}$, b_{-I}, and b_{+I} are the saturation capacity and the equilibrium constants of nicotinate and nicotinium species.

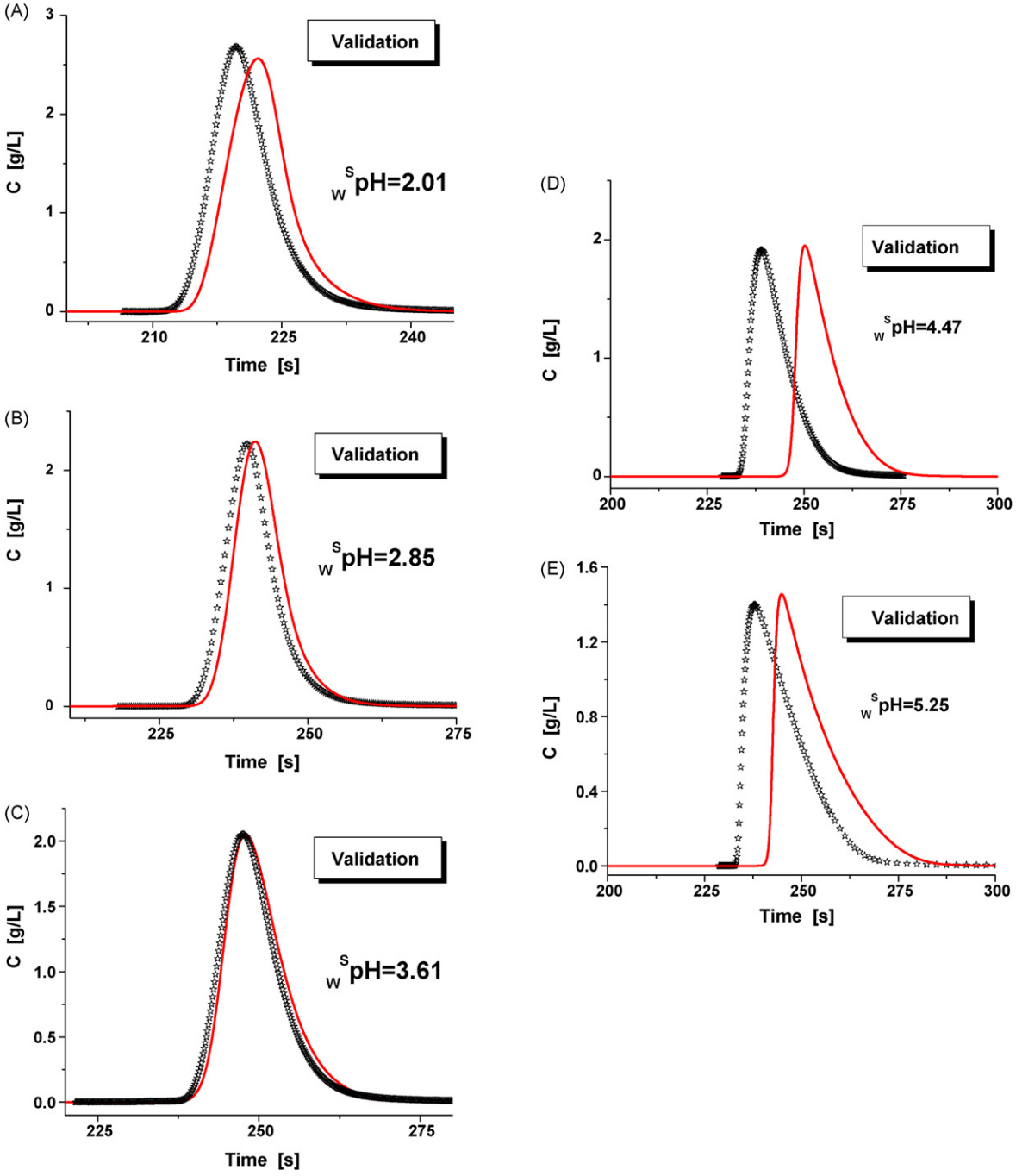

Fig. 9. Comparison between the experimental (dashed lines) and the calculated (solid lines) band profiles of nicotinic acid at five different mobile phase $^{S}_{W}$pHs. Note the excellent prediction of the band shape and the validity of the general adsorption isotherm model Eq. (15).

4.4.2. Adsorption of the nicotinate species

The isotherm parameters of nicotinate ($q_{S,I}$ and b_{-I}) were estimated by the inverse method, as those giving the best agreement between the experimental overloaded band profile recorded at ${}^{S}_{W}\text{pH} = 6.11$ (injection of 30 mM sodium nicotinate) and the calculated profile (see Fig. 8A). The adsorption of nicotinium in Eq. (15) was neglected ($\alpha_{+I} \simeq 0$). The molar compositions α_0 and α_{-I} were determined at various concentrations C_T by solving the thermodynamic problem in the bulk phase. We found $q_{S,I} = 1.93$ g/L and $b_{-I} = 0.32$ L/g. Possibly, the carboxylate group of nicotinate can be involved in hydrogen-bonding interactions with the proton of the accessible silanol groups at ${}^{S}_{W}\text{pH} = 6.11$.

4.4.3. Adsorption of the nicotinium species

The only remaining isotherm parameter of nicotinium (b_{+I}) was estimated at ${}^{S}_{W}\text{pH} = 1.37$ (after injection of 50 μL of a 30 mM solution of nicotinic acid in this buffer), hence $q_{S,+I} = 1.93$ g/L. The best agreement between experimental and calculated band profiles (see Fig. 8B) is found with $b_{+I} = 0.048$ L/g. The band profiles are apparently anti-Langmuirian because the ratio of the concentrations of nicotinium to nicotinic acid decreases with increasing total concentration of the injected sample (the zwitterionic form was injected). We observed that the negatively charged species (nicotinate) interacts more strongly with the active sites ($q_{S,I}$) than the positively charged species (nicotinium). Our thermodynamic results do not permit any direct conclusion regarding the retention mechanisms. This reservation made, it is not unreasonable to suggest that residual silanol groups of the derivatized and endcapped X-bridge silica could be protonated at ${}^{S}_{W}\text{pH} = 1.37$, inducing repulsion of the positively charged ions from the adsorption sites of type I. At least this suggestion is consistent with thermodynamic results.

4.4.4. Validation of the general adsorption isotherm for nicotinic acid

Fig. 9A–E compare the experimental and calculated band profiles of nicotinic acid (50 μL of a 30 mM sample solution in the buffer solution) when using the buffer solutions II (${}^{S}_{W}\text{pH} = 2.01$), III (${}^{S}_{W}\text{pH} = 2.85$), IV (${}^{S}_{W}\text{pH} = 3.61$), V (${}^{S}_{W}\text{pH} = 4.47$), and VI (${}^{S}_{W}\text{pH} = 5.25$). The isotherm parameters previously estimated are listed in Table 5. All the molar composition α_i were calculated by solving the bulk thermodynamic problem. We note an excellent agreement between the shapes of the recorded and calculated band profiles. Accordingly, the general adsorption isotherm Eq. (15) accounts well for the adsorption of nicotinic acid at all pHs, for a constant ionic strength of 0.1 M. Nevertheless, we note variable degrees in the shift of the position of the calculated band profiles with respect to the position of the experimental band profiles. This could suggest that the pK_as of nicotinic acid in pure water are somehow different of those in the 10/90 solution of methanol in water, which could affect the calculation of the molar fractions α_i in the bulk mobile phase.

5. Conclusion

The overloaded band profiles of phthalic and nicotinic acid, which have two acido-basic functions, hence may exist in solutions under three possible forms, eluted in mobile phases at pHs increasing from below the smaller pK_a to above the larger one were successfully predicted on a commercial X-Bridge C_{18} column. The ionic strength was kept nearly constant at 0.1 M. The calculated band profiles were derived from the following assumptions:

1. The composition of the bulk solution was calculated using the Debye–Hückel theory in order to estimate the activity coefficients of the three species in the bulk mobile phase.
2. A bi-Langmuir isotherm (two types of sites, 1 and 2) was assumed for the adsorption of the neutral species (including the zwitterionic one) and a competitive Langmuir adsorption model for the adsorption of the ionic species (one type of sites, I). The competition for adsorption between the neutral and the ionic species was assumed to be negligible.
3. The simple equilibrium-dispersive model of chromatography was used to calculate the concentration band profiles.

A physical description of the properties of the adsorption sites 1, 2, and I can be given. Sites of type 1 involve dispersive interactions and have the lowest adsorption energy. They are located at the interface between the tip of the C_{18}-bonded layer and the bulk mobile phase. The saturation capacity $q_{S,1}$ can easily be estimated from the characteristics of the adsorbent, of the packed column, and from the density and molecular weight of the pure neutral compound. Sites of type 2 have a higher adsorption energy than sites of type 1. They are located deeper amidst the C_{18}-bonded chains. The smaller the size of the neutral compound, the larger the saturation capacity $q_{S,2}$ of these sites. The interactions between analyte and stationary phase on these sites are also dispersive. Ionizable compounds adsorb weakly onto sites 1 and 2, which allows the competition for adsorption onto these sites between the neutral and any ionizable forms of an acido-basic compound to be neglected.

Finally, the sites of type I are specific to ionic compounds. Their density is much less than that of sites of types 1 or 2, by one to two order of magnitude. Our results show that nicotinate is strongly bound to these sites at ${}^{S}_{W}\text{pH} = 6$ while nicotinium interacts less strongly with them at ${}^{S}_{W}\text{pH} = 1.5$. Also, our results show that the doubly charged anion phthalate II is not retained on these sites, probably because this highly polar anion is strongly repelled from the C_{18} environment. So far, a plausible explanation for these sites I is the presence of unreacted but accessible silanol groups at the silica surface. Neutral species do not significantly adsorb on these sites because water and methanol, which are present in large amounts in the bulk are preferentially adsorbed onto them. Singly charged sample molecules can still access them and interact through charge–dipole interactions with the Si-O(δ^-)H(δ^+) groups.

The present work should help to predict the elution band profiles of small peptides which have at least two pK_as. The application of this work to preparative chromatography of small peptides under selected pH and ionic strength conditions is in progress, using our general model of adsorption under RPLC condition for any pH and ionic strength of the bulk phase. As the number of amino-acid in the peptide sequence increases, a large distribution of pK_a values is expected to take place, and the net charge of the peptide will become the critical parameter in the prediction of the retention behavior of biomolecules in RPLC.

Finally, the microscopic description (multi-Langmuir adsorption isotherm) of the adsorption behavior of acido-basic compounds that we have presented should be considered with caution. While the experimental results reported are valid because based on the whole body of chemical thermodynamics and on acknowledged methods of measurements that have been amply validated, they could be interpreted using other adsorption models, for example those based on surface potentials, which have had a tremendous impact on our understanding of the adsorption of electrolytes in electrochemistry and in colloidal stability. As stated in the introduction, adsorption data obtained with either frontal analysis or the inverse method of chromatography cannot provide a microscopic description of the adsorption process. They merely inform on the degree of heterogeneity of the adsorption process, the equilibrium constants involved, and the saturation capacities of the column. Microscopic interpretations derived from

these observations are speculative and should be used to orient in the design of experiments that could confirm or falsify these suggestions.

Acknowledgements

This work was supported in part by grant CHE-06-08659 of the National Science Foundation and by the cooperative agreement between the University of Tennessee and the Oak Ridge National Laboratory.

References

[1] N.H. Davies, M.R. Euerby, D.V. McCalley, J. Chromatogr. A 1119 (2006) 11.
[2] D.V. McCalley, J. Chromatogr. A 1075 (2005) 57.
[3] N.H. Davies, M.R. Euerby, D.V. McCalley, J. Chromatogr. A 1178 (2008) 71.
[4] U.D. Neue, C.H. Phoebe, K. Tran, Y.-F. Cheng, Z. Lu, J. Chromatogr. A 925 (2001) 49.
[5] J. Samuelsson, A. Franz, B.J. Stanley, T. Fornstedt, J. Chromatogr. A 1163 (2007) 177.
[6] L. Pan, R. LoBrutto, Y.V. Kazakevich, R. Thompson, J. Chromatogr. A 1049 (2004) 63.
[7] F. Gritti, G. Guiochon, Anal. Chem. 75 (2003) 5726.
[8] F. Gritti, G. Guiochon, Anal. Chem. 78 (2006) 5823.
[9] F. Gritti, G. Guiochon, J. Chromatogr. A 1099 (2005) 1.
[10] J.L. Rafferty, J.I. Siepmann, M.R. Schure, Anal. Chem. 80 (2008) 6214.
[11] F. Gritti, G. Guiochon, J. Sep. Sci. 31 (2008) 3657.
[12] F. Gritti, G. Guiochon, J. Chromatogr. A 1216 (2009) 63.
[13] F. Gritti, G. Guiochon, J. Chromatogr. A 1216 (2009) 1776.
[14] K.N. Chattoraj, K.S. Birdi, Adsorption and the Gibbs Surface Excess, Plenum, New York, NY, 1984.
[15] A.J. Bard, L.R. Faulkner, Electrochemical Methods: Fundamentals and Applications, 2nd ed., John Wiley and Sons, Inc., New York, NY, 2001, p. 534.
[16] J. Stahlberg, J. Chromatogr. A 855 (1999) 3.
[17] F. Gritti, G. Guiochon, J. Chromatogr. A 1216 (2009) 3175.
[18] A. Andrzejewska, F. Gritti, G. Guiochon, J. Chromatogr. A 1216 (2009) 3992.
[19] E. Bosch, P. Bou, H. Allemann, M. Rosés, Anal. Chem. 68 (1996) 3651.
[20] K.N. Han, Fundamentals of Aqueous Metallurgy, SME, Littleton, CO, 2002, p. 73.
[21] K.S. Kanse, S.D. Chavan, C.S. Mali, A.C. Kumbarkhane, S.C. Mehrotra, Indian J. Phys. 80 (2006) 265.
[22] E. Subirats, M. Rosés, E. Bosch, Sep. Purif. Rev. 36 (2007) 231.
[23] P.I. Nagy, K. Takacs-Novak, J. Am. Chem. Soc. 68 (1996) 3651.
[24] Handbook of Chemistry and Physics, 68th ed., CRC Press, Boston, MA, 1987.
[25] G. Guiochon, S.G. Shirazi, A. Felinger, A.M. Katti, Fundamentals of Preparative and Nonlinear Chromatogrtaphy, Academic Press, Boston, MA, 2006.
[26] P.W. Dankwerts, Chem. Eng. Sci. 2 (1953) 1.
[27] K. Kaczmarski, M. Mazzotti, G. Storti, M. Morbidelli, Comput. Chem. Eng. 21 (1997) 641.
[28] K. Kaczmarski, Comput. Chem. Eng. 20 (1996) 49.
[29] K. Kaczmarski, D. Antos, J. Chromatogr. A 862 (1999) 1.
[30] A. Felinger, A. Cavazzini, G. Guiochon, J. Chromatogr. A 986 (2003) 207.
[31] F. Gritti, A. Felinger, G. Guiochon, J. Chromatogr. A 1017 (2003) 45.
[32] F. Gritti, A. Felinger, G. Guiochon, J. Chromatogr. A 995 (2003) 37.
[33] M. Jaroniec, R. Madey, Physical Adsorption on Heterogeneous Solids, Elsevier, Amsterdam, 1988.